

Second-Order Jahn–Teller Instability and the Activation Energy for $\text{Al}^+(^1S) + \text{H}_2 \rightarrow \text{AlH}^+(^2\Sigma^+) + \text{H}$

JON RUSHO, JEFF NICHOLS,* AND JACK SIMONS

Chemistry Department, University of Utah, Salt Lake City, Utah 84112

Abstract

The interaction of $\text{Al}^+(^1S)$ ions with H_2 on the lowest electronic energy surface is studied using *ab initio* electronic structure methods. A C_s symmetry transition state is located and found to have the geometry of a product AlH^+ ion loosely bound to a H atom, consistent with the Hammond postulate for this endothermic reaction. Locating this transition state, beginning at geometries that characterize vibrationally cold H_2 and translationally hot Al^+ , posed special challenges to the commonly used “hill-climbing” algorithm because of regions of geometrical instability along the path thus generated. This instability was found to be a result of second-order Jahn–Teller coupling with a low-lying 1B_2 electronic state. In addition to these primary findings, a weakly bound T-shaped $\text{Al}^+ \cdots \text{H}_2$ C_{2v} van der Waals complex is found that lies only 242 cm^{-1} below the Al^+ and H_2 asymptote, with H–H internuclear separation only slightly distorted from the equilibrium bond distance of H_2 and an Al–H distance (3.5 \AA) much longer than the covalent bond length in AlH^+ (1.6 \AA). The locally stable but thermodynamically unstable linear $\text{HAlH}^+(^1\Sigma_g^+)$ species and, of course, the $\text{H} + \text{AlH}^+(^2\Sigma^+)$ reaction products have also been identified as critical points on the ground-state surface. Where known, the geometries and energies that we calculate agree well with experimental data. © 1993 John Wiley & Sons, Inc.

I. Introduction

Our earlier theoretical calculations [1, 2] on $\text{B}^+ + \text{H}_2 \rightarrow \text{BH}^+ + \text{H}$ and other such ion–molecule reactions in which both reactants have closed-shell ground electronic states as well as recent experimental data [3] on B^+ , Al^+ , and Ga^+ interacting with H_2 prompted our study of $\text{Al}^+ + \text{H}_2$. In particular, Armentrout et al [3a, b], in guided ion-beam measurements, found an energy threshold to $\text{AlH}^+ + \text{H}$ formation of ca. 6.5 eV or 150 kcal/mol, which is *much* higher than the thermodynamic threshold (i.e., reaction endothermicity) of about 3.9 eV (91 kcal/mol). The large discrepancy between the endothermicity and observed product-formation threshold prompted this study.

Although the most likely explanation for the discrepancies relevant to the ion-beam experiment has already been provided by us [2] in terms of collision-to-internal energy transfer, the work on AlH_2^+ discussed here produced additional insights into so-called hill-climbing procedures that are commonly employed for locating transition states starting from reactant geometries. These difficulties and a device found useful in overcoming them are thus the primary focus of this paper.

*Present address: Pacific Northwest Laboratories, Richland, WA.

II. Computational Methods

A. Atomic Orbital Basis Sets

The basis set for the H atoms consists of the Dunning augmented correlation consistent (cc) polarized valence triple-zeta [$5s2p1d/3s2p1d$] set [4] of functions. For the Al^+ ion, the McLean–Chandler [$12s9p/6s5p$] basis [5] with a d -polarization function with an exponent of 0.4 was used. A total of 54 contracted Gaussian-type basis functions resulted. These same bases have been used in our earlier works on B^+ , Al^+ , and Ga^+ and have proven reliable as further illustrated below.

B. Electronic Configurations and Wave Functions

Complete active space multiconfigurational self-consistent field (CAS–MCSCF) methods were used to generate the lowest 1A_1 and 1B_2 electronic states of the $Al^+ + H_2$ system in C_{2v} symmetry. All molecular orbitals derived from the two H $1s$ orbitals and the Al^+ ion's $3s$ and $3p$ orbitals were included in the active orbital space, and the four valence electrons were distributed among these orbitals in all possible ways consistent with the specified symmetry. These MCSCF calculations were carried out using our in-house Utah MESSKit program suite.[†]

By applying our analytical energy derivative and potential energy surface walking and hill-climbing algorithms [6], we were able to find and characterize (via energy, geometry, and local harmonic vibrational frequencies) various local minima on the ground-state potential energy surface. Some of these minima correspond to weakly bound van der Waals complexes, and others, to chemically bound minima. At each such critical point, we used more correlated methods to obtain more accurate values for the correlation energies. In particular, we employed the QCISD(T) method [7].

By monitoring the location of the lowest excited singlet state (the 1B_2 state in C_{2v} symmetry), we were able to also identify the origin of the instability on the 1A_1 ground-state surface, as discussed below.

C. Surface Exploration Strategy

Knowing the geometries of the reactant ($Al^+ + H_2$) species and bearing in mind that the experiments [3] involve vibrationally cold H_2 molecules, we employed a hill-climbing algorithm to move uphill in energy, starting by moving along an eigenmode of the second-derivative (Hessian) matrix corresponding to the Al^+ -to- H_2 relative motion. This triatomic species has only three eigenmodes of non-zero frequency: the high-frequency H—H stretch, the Al^+ to H_2 radial motion mode, and the $Al^+ \cdots H_2$ asymmetric stretch (or H_2 hindered rotation) mode. Following the radial motion mode makes good chemical sense, although, as we show later, it does *not* produce a valid reaction path.

[†]The Utah MESS-KIT is a suite of highly modular codes that were programmed in-house to give a variety of electronic functionalities by J. A. Nichols, M. R. Hoffmann, R. A. Kendall, H. L. Taylor, D. W. O'Neal, E. Earl, R. Hernandez, M. Gutowski, J. Boatz, K. Bak, J. Anchell, X. Wang, M. Feyereisen, and J. Simons.

In hill-climbing algorithms, one moves "uphill" (in the potential energy topography) along one Hessian eigenmode while minimizing the potential energy with respect to all $3N - 7 = 2$ (in this case) orthogonal coordinates. For this reason, one often speaks of progressing uphill along a "stream bed." When applied to the $\text{Al}^+ + \text{H}_2$ surface, the act of minimizing along the H—H and $\text{Al}^+ \cdots \text{H}_2$ asymmetric stretch modes produce C_{2v} structures at which (i) the gradient has a component only along the Al^+ -to- H_2 radial mode and (ii) all $3N - 6 = 3$ Hessian eigenvalues are (at least at early stages of the hill-climbing process) positive. It is not at all surprising that C_{2v} structures result from this algorithm because the charge-quadrupole interaction between Al^+ and H_2 favors placing the Al^+ ion in regions of higher electron density.

In the following sections of this paper, we describe the outcome of following this hill-climbing algorithm from the early stage C_{2v} geometries discussed above, ultimately to the transition state. Anticipating one of our primary findings, we emphasize now that one is by no means guaranteed that such a process will lead to a transition state, nor is one guaranteed that the path traced by this process is a conventional reaction path [8]. In fact, as shown below, the hill-climbing algorithm encounters problems involving symmetry breaking that require introducing a new device to overcome. Moreover, because the transition state ultimately located has C_s symmetry (which we did not know beforehand), the particular hill-climbing approach used here could *not possibly* trace out a path identical to the conventional reaction path because the reaction coordinate is known to be symmetry-preserving [8], i.e., any path connecting the early stage C_{2v} geometries of our hill-climbing process to the eventual C_s -symmetry transition state *must* (unless the electronic state becomes degenerate) involve symmetry-lowering, so that the path we traced to find the transition state cannot be a true reaction path. This means that there exists a lower-energy path leading from the C_s transition state to the $\text{Al}^+ + \text{H}_2$ reactants that does *not* involve C_{2v} symmetry. It remains a significant challenge to imagine an algorithm that *begins* at $\text{Al}^+ + \text{H}_2$ geometries and traces such a path *uphill*.

Although the above discussion shows that starting our search for a transition state at C_{2v} geometries can lead along a path that cannot connect to the true reaction path, the hill-climbing algorithm employed here is widely used and, in our opinion, provides a useful tool for exploring candidate stream beds that may or may not lead to a transition state. If one eventually succeeds in locating a transition state, it is then wise to begin a "downhill" walk at that point and to thus trace out the true [8] reaction path; in the $\text{Al}^+ + \text{H}_2$ case at hand, doing so does not lead to C_{2v} geometries.

Having now made it clear why we initially chose to explore C_{2v} (and near- C_{2v}) symmetry and to follow the Al^+ -to- H_2 radial mode uphill, let us now summarize the primary "topographical features" encountered along this hill-climbing adventure.

III. Findings

A. Special Points on the 1A_1 and 1B_2 Surfaces

In Table I, we summarize the primary energetic results of our calculations for various species and critical points on the lowest single-state surface, many of which are subject to experimental verification. Clearly, our relative placement of the $^{1,3}P$

TABLE I. Energies (kcal/mol) measured with respect to $\text{Al}^+(^1S) + \text{H}_2(^1\Sigma_g^+)$.

Species	This work ^b	Experiment ^a
$\text{Al}^+(^1S) + \text{H}_2(^1\Sigma_g^+)$	0.0	0.0
$\text{Al}^+(^1S) + 2\text{H}(^2S)$	109	110
$\text{Al}^+(^3P) + \text{H}_2(^1\Sigma_g^+)$	105	107
$\text{Al}^+(^1P) + \text{H}_2(^1\Sigma_g^+)$	180	171
$\text{AlH}^+(^2\Sigma) + \text{H}$	$\Delta E_{\text{Thermo.}} = 91$	
$\text{HAlH}^+(^1\Sigma_g^+)$	12	
$\text{Al}^+ \cdots \text{H}_2$ C_{2v} barrier	104	
Onset of b_2 instability	92	
Al^+H_2 C_s transition state	95	

^a[9].^bBased on QCISD(T) data except for 1P state where projected fourth-order Møller–Plesset (PMP4) perturbation theory was used due to difficulties in the QCISD(T) convergence.

states of Al^+ and of the $\text{H} + \text{H}$ asymptote are in good agreement with what is known experimentally. Unfortunately, the energies of linear HAlH^+ and of $\text{AlH}^+ + \text{H}$ are not yet well characterized experimentally, so we cannot further calibrate our computations with comparisons to experimental data for them.

In Table II, we provide further data (absolute energies, geometries, local harmonic vibrational frequencies) relative to the species treated in Table I, as well as information about other especially important species: (i) C_{2v} and linear van der Waals complexes, (ii) the minimum-energy structure of the excited 1B_2 electronic state that derives from $\text{Al}^+(^1P) + \text{H}_2$, (iii) the location on the 1A_1 ground-state energy surface at which b_2 mode (i.e., asymmetric stretch) geometrical instability first occurs, and (iv) the transition state of C_s symmetry found on the ground electronic state surface.

Although the C_{2v} van der Waals complex should be amenable to study as an intact entity in, e.g., supersonic beams, the linear complex is geometrically unstable with respect to bending. Neither is of special relevance to our efforts to understand the thermal reaction threshold for $\text{Al}^+ + \text{H}_2 \rightarrow \text{AlH}^+ + \text{H}$, although the former could be a starting point for future thermal reaction rate measurements of $\text{AlH}_2^+ + \text{H}_2 \rightarrow \text{AlH}^+ + \text{H}$, although the former could be a starting point for future thermal reaction rate measurements of $\text{AlH}_2^+ \rightarrow \text{AlH}^+ + \text{H}$.

B. Relevance to $\text{Al}^+ + \text{H}_2$ Reaction

At collision energies of ca. 6.5 eV (i.e., ca. 150 kcal/mol), which corresponds to the observed experimental threshold for producing $\text{AlH}^+ + \text{H}$ from $\text{Al}^+ + \text{H}_2$, other species (e.g., HAlH^+ , and $\text{Al}^+ + \text{H} + \text{H}$) are also accessible, as are the 1B_2 excited state and the region on the 1A_1 surface where negative curvature along the b_2 mode occurs. Let us therefore examine in more detail the most likely fate of collisions whose initial flux describes $\text{Al}^+(^1S) + \text{H}_2$ on the 1A_1 surface at collision energies in excess of the ca. 91 kcal/mol endothermicity, approaching and then exceeding 6.5 eV.

TABLE II. Total and relative energies, geometries, and vibrational frequencies for species relating to the $\text{Al}^+ + \text{H}_2 \rightarrow \text{AlH}^+ + \text{H}$, HAlH^+ reactions.

Species	Electronic energies (Hartrees)	Optimized Internuclear Distances (Å)	Vibrational frequencies ^b /zero-point energies (cm^{-1})	Relative energies (kcal/mol) ^a
$\text{Al}^+(^1S) + \text{H}_2$	-242.856705 -242.879646	$r = 0.755$	4224/2112	0.0 0.0
$\text{AlH}^+(^2\Sigma) + \text{H}$	-242.717076 -242.735419	$r_{\text{AlH}} = 1.658$	1424/712	88 91
$\text{HAlH}^+(^1\Sigma_g^+)$	-242.804625 -242.860474	$r = 3.103$	1940(a_1) 2055 (b_2) 513 (bend)/ 2511	33 12
$\text{Al}^+ \cdots \text{H}_2$ barrier	-242.692731 -242.713641	$r = 1.852$ $R = 1.587$	2362 i (a_1) 1942 i (b_2) 996 (a_1)	103 104
$\text{Al}^+ \cdots \text{H}_2$ C_{2v} complex	-242.857807	$r = 0.76$ $R = 3.45$	4199 (a_1) 270 (a_1) 106 (b_2)/ 2288	-242 cm^{-1}
$\text{H—H} \cdots \text{Al}^+$ linear complex	-242.856718	$r = 0.76$ $R_{\text{Al—H}} = 3.67$	4224 (σ) 48 (σ) 203 i (π)	3 cm^{-1}
AlH_2^+ (1B_2) minimum	-242.685868 -242.740915	$r = 1.729$ $R = 1.429$	855 (a_1) 1307 (b_2) 1637 (a_1)/ 1900	107 87
Onset of b_2 -mode instability	-242.705739 -242.733423	$r = 1.69$ $R = 1.59$	2087 i (a_1) 1096 (a_1) 821 i (b_2)	95 92
C_s transition state	-242.717327 -242.727637	$r_{\text{AlH}_1} = 4.04$ $r_{\text{AlH}_2} = 1.66$ $r_{\text{H}_1\text{H}_2} = 3.39$	1420 85 112 i / 753	88 95

^aIn all cases, the energies are given relative to the $\text{Al}^+ + \text{H}_2$ reactants. These are electronic energies and thus do not include zero-point corrections. In each case, and for the column giving total energies in Hartrees, the first number is based on our CAS–MCSCF calculations and the second is based on our QCISD(T) data.

^bThese local harmonic frequencies were obtained from the analytical second derivatives of the MCSCF energy at the MCSCF geometries.

In Figure 1 we show a C_{2v} symmetry contour plot of the ground electronic state energy surface for AlH_2^+ with the energies given in kcal/mol relative to $\text{Al}^+ + \text{H}_2$, and the axes being r (the H—H distance in Å) and R (the Al^+ to center of H—H distance in Å). Here, the narrow entrance channel along which $r \approx 0.76$ Å is evident.

Flux moving up this channel experiences repulsive forces along the R coordinate and very little coupling (i.e., as measured by the cross terms $\partial^2 E / \partial r \partial R$ on this surface) between the R and r coordinates. Except as specified in the following paragraph, the energy surface along the b_2 coordinate, which is not shown in this figure, has positive curvature that acts to retain C_{2v} symmetry as the hill-climbing algorithm progresses.

Figure 2 shows this same surface in three-dimensional form, along with the excited 1B_2 surface as a function of these same two C_{2v} -symmetry-preserving coordinates (r and R). Clearly, as the Al^+ ion approaches the H_2 molecule closely, the closed-shell nature of both species causes the ground-state surface to become quite repulsive. In contrast, the $3s^1 3p^1$ nature of the excited Al^+ ion allows for attractive interaction with H_2 because the $\text{Al}^+ 3s$ orbital can accept electron density from the occupied σ_g orbital of H_2 while the b_2 -symmetry $3p$ orbital of Al^+ can donate density into the empty σ_u orbital of H_2 . These Al^+ -to- H_2 attractive interactions also lead to weakening of the $\text{H}-\text{H}$ bond in H_2 because the σ_u orbital acquires electron density. It is clear from Figure 2 that the 1A_1 and 1B_2 surfaces are nearly isoenergetic in regions close to where the barrier occurs on the 1A_1 surface, so it is essential to further explore any couplings between these surfaces.

In Figure 3 we show a portion of the 1A_1 ground-state surface in a region where the 1B_2 surface is quite close in energy. At each of the grid points shown, we also evaluated the curvature of the 1A_1 energy function along the symmetry-breaking b_2 mode. At those points marked by the diamond shape, this curvature was found to be negative; at points not so marked, the curvature was positive as a result of which C_{2v} geometry tends to be retained (by positive restoring forces) in the hill-climbing

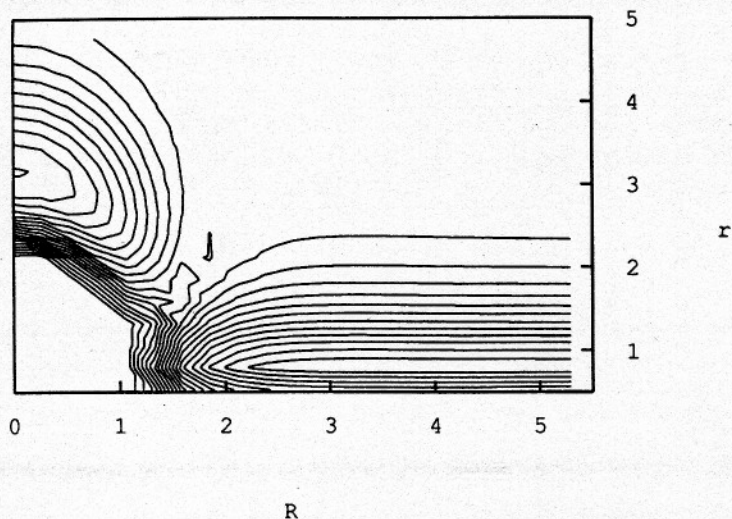


Figure 1. C_{2v} symmetry contour plot of the (1A_1) ground-state energy of $\text{Al}^+ + \text{H}_2$. The R (distance of Al^+ to the center of $\text{H}-\text{H}$) and r ($\text{H}-\text{H}$ distance) axes are in \AA , and the contours are spaced by 10.6 kcal/mol.

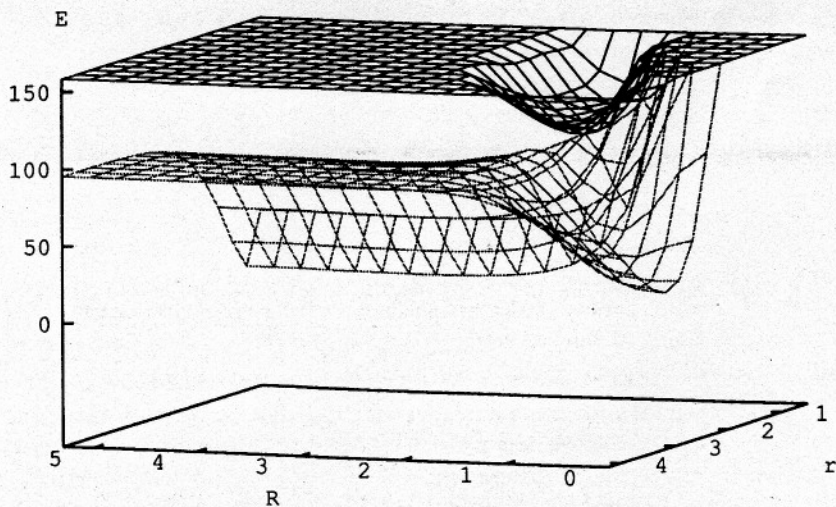


Figure 2. The same 1A_1 AlH_2^+ energy surface as given in Figure 1 shown in three dimensions; portions of the lowest 1B_2 surface are also shown (regions of the 1B_2 surface have been truncated when in excess of 150 kcal/mol).

process. The lowest energy-point at which negative b_2 -mode curvature occurs is at $r = 1.69 \text{ \AA}$ and $R = 1.59 \text{ \AA}$, where the electronic energy on the ground-state surface is 92 kcal/mol above $\text{Al}^+ + \text{H}_2$ and the b_2 -mode frequency is $821 i \text{ cm}^{-1}$. At this point, the two a_1 symmetry nodes have local harmonic frequencies of $2087 i \text{ cm}^{-1}$

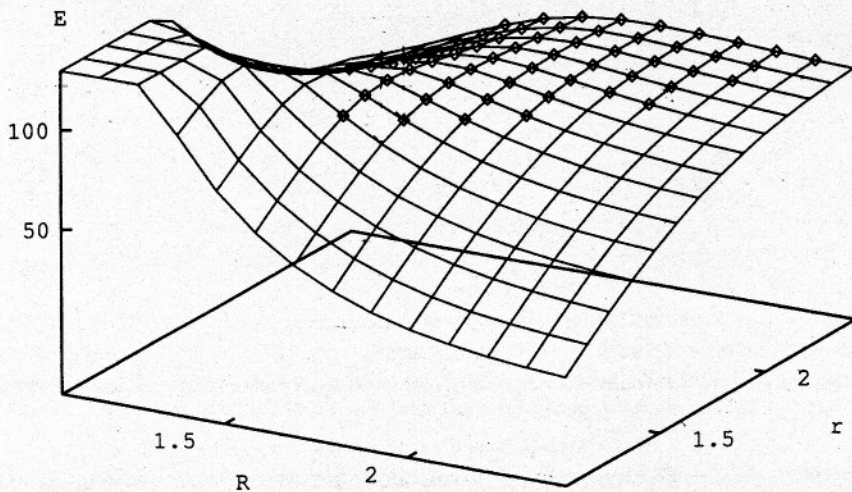


Figure 3. The 1A surface in a region where the 1B_2 surface is very close to it. At grid points marked by the diamond shape, the b_2 -mode local vibrational frequency is imaginary (and denoted by a negative value where shown); at other points, it is real.

and 1096 cm^{-1} , the latter being the HAlH^+ bending motion, and the former, the Al^+ -to- H_2 relative motion.

It should be noted that the point at which the b_2 -mode instability first sets in (i.e., the onset point for second-order Jahn-Teller [SOJT] instability) has one imaginary frequency and one (nearly) zero frequency; the former is the Al^+ -to- H_2 motion, and the latter, the b_2 -mode distortion. Moreover, the gradient at this point does *not* vanish, but is quite substantial. This means that this point is *not* a transition state; conventional transition states possess one imaginary frequency coordinate with all other local harmonic vibrational frequencies being positive.

However, it can be shown [10] that the energy at this point is (nearly) equal to that of a nearby point of lower symmetry whose geometry differs from that of the SOJT onset point by a distortion along the b_2 -mode of magnitude $\delta b_2 = \sqrt{-F/(A_{b_2})}$. Here, F is the magnitude of the gradient at the SOJT point and A_{b_2} is related to the rate of change of the curvature along the b_2 mode with respect to movement along the coordinate along which the gradient lies [10]: $A_{b_2} = 1/2[\partial/(\partial R)][(\partial^2 E)/(\partial b_2^2)]$. We can, of course, evaluate A_{b_2} given the b_2 -mode frequency data embodied in Figure 3. Doing so gives $A_{b_2} = 0.40$ Hartree/bohr³. Then, using the value of the gradient $F = 0.11$ Hartree/bohr at the point of b_2 -mode instability produces, via the above equation, $\delta b_2 = 0.52$ bohr, which amounts to a "twist" of the H—H axis by ca. 19° relative to the C_{2v} geometry.

After effecting such a 19° "twist," we found that only one eigenvalue of the Hessian matrix was then negative and the gradient was smaller than at the point of b_2 -mode instability (although not vanishingly small as the model developed in [10] suggests). Subsequently, following this negatively curved eigenmode using our hill-climbing strategy [6], we located the C_s -symmetry transition state described in Table II. This transition state lies ca. 95 kcal/mol above the reactants and ca. 3 kcal/mol above the point of SOJT instability and has a geometry very close to that of AlH^+ weakly interacting with a quite distant H atom.

IV. Overview and Summary

The reaction $\text{Al}^+ + \text{H}_2 \rightarrow \text{AlH}^+ + \text{H}$ is endothermic by ca. 91 kcal/mol, and the metastable linear HAlH^+ ion lies 12 kcal/mol above $\text{Al}^+ + \text{H}_2$ (both energies being without zero-point corrections; see Table II). A C_s symmetry transition state, whose geometry is close to that of AlH^+ with a weakly attached H atom, is found to lie 95 kcal/mol above the $\text{Al}^+ + \text{H}_2$ reactants.

Because the transition state has lower symmetry than that used to *begin* the hill-climbing process from the $\text{Al}^+ + \text{H}_2$ reactants, the algorithm used was doomed to *not* produce a true reaction path. Nevertheless, the strategy of hill climbing, supplemented by a device that suggest how to move *away* from C_{2v} symmetry, did succeed in locating the C_s transition state. Although one would prefer to have a process that begins with $\text{Al}^+ + \text{H}_2$ and progress *uphill* along the proper (C_s , *not* C_{2v}) reaction path, we are not presently aware of such a procedure. In its absence, we suggest that the hill-climbing method used here (and widely used elsewhere), *supplemented*

by the symmetry-lowering tool employed here, provides a useful approach to finding transition states if not reaction paths.

Acknowledgments

This work was supported in part by the Office of Naval Research and by National Science Foundation Grant #CHE9116286. We also wish to thank Prof. Mark Gordon and Dr. Gregory J. Atchity of Iowa State University whose graphical analysis of our analogous $B^+ + H_2$ energy surface provided insights that allowed us to locate the C_s -symmetry transition state found in this work; without their help, this work likely would have remained unfinished.

Bibliography

- [1] J. Nichols, M. Gutowski, S. J. Cole, and J. Simons, *J. Phys. Chem.* **96**, 644 (1992).
- [2] M. Gutowski, M. Roberson, J. Rusho, J. Nichols, and J. Simons, *J. Chem. Phys.* **99**, 2601 (1993).
- [3] (a) P. B. Armentrout, *Int. Rev. Phys. Chem.* **9**, 115 (1990). (b) J. L. Elkind and P. B. Armentrout, (unpublished results).
- [4] T. Dunning, *J. Chem. Phys.* **90**, 1007 (1989).
- [5] A. D. McLean and G. S. Chandler, *J. Chem. Phys.* **72**, 5639 (1980).
- [6] J. Nichols, H. Taylor, P. Schmidt, and J. Simons, *J. Chem. Phys.* **92**, 340 (1990); J. Simons, P. Jørgensen, H. Taylor, and J. Ozment, *J. Phys. Chem.* **87**, 2745 (1983); D. O'Neal, H. Taylor, and J. Simons, *J. Phys. Chem.* **88**, 1510 (1984); A. Banerjee, N. Adams, J. Simons, and R. Shepard, *J. Phys. Chem.* **89**, 52 (1985); H. Taylor and J. Simons, *J. Phys. Chem.* **89**, 684 (1985); C. J. Cerjan and W. H. Miller, *J. Chem. Phys.* **75**, 2800 (1981); J. Baker, *J. Comp. Chem.* **9**(5), 465 (1988); J. Baker, *J. Comp. Chem.* **7**(4), 385 (1986).
- [7] M. J. Frisch, M. Head-Gordon, G. W. Trucks, J. B. Foresman, H. B. Schlegel, K. Raghavachari, M. A. Robb, J. S. Binkley, C. Gonzales, D. J. DeFrees, D. J. Fox, R. A. Whiteside, R. Seeger, C. F. Melius, J. Baker, R. L. Martin, L. R. Kahn, J. J. P. Stewart, S. Topiol, and J. A. Pople, *Gaussian 90* (Gaussian Inc., Pittsburgh, PA, 1990).
- [8] J. Simons, *Energetic Principles of Chemical Reactions* (Jones and Bartlett, Portola Valley, CA, 1983); R. G. Pearson, *Symmetry Rules for Chemical Reactions* (Wiley, New York, 1976).
- [9] C. E. Moore, *Tables of Atomic Energy Levels* (U.S. Govt. Printing Office, Washington, D.C., 1971). K. P. Huber, G. Herzberg, *Molecular Spectra and Molecular Structure, IV, Constants of Diatomic Molecules* (Van Nostrand Reinhold, New York, 1979).
- [10] J. Simons, *Int. J. Quantum Chem.* (in press).

Received May 25, 1993

Revised manuscript received July 13, 1993

Accepted for publication July 20, 1993